

## RESEARCH ARTICLE

View Article Online

View Journal | View Issue

Cite this: *Org. Chem. Front.*, 2022, **9**, 64

## Sequence-sorted redox-switchable hetero[3]rotaxanes†

Marius Gaedke,<sup>†a</sup> Henrik Hupatz,<sup>†a</sup> Felix Witte,<sup>†b</sup> Susanne M. Rupf,<sup>†c</sup> Clara Douglas,<sup>†a</sup> Hendrik V. Schröder,<sup>†a</sup> Lukas Fischer,<sup>a</sup> Moritz Malischewski,<sup>†c</sup> Beate Paulus<sup>†b</sup> and Christoph A. Schalley<sup>†\*a</sup>

From a library of five crown ether macrocycles with different ring sizes and redox-active moieties, such as tetrathiafulvalene (TTF) and naphthalene diimide (NDI), directional heterocircuit[3]rotaxanes were constructed. Using an axle with two binding sites with different steric accessibility, the concept of integrative self-sorting was applied to program the sequence of functional units in heteropseudo[3]rotaxanes. Depending on binding strength and ring size of the smaller macrocycles, different heteropseudo[3]rotaxane selectivities and stabilities were determined by 2D NMR spectroscopy and tandem mass spectrometry. A heteropseudo[3]rotaxane with rotaxane-like behaviour was isolated chromatographically, displaying electrochemically “frustrated” properties. A robust synthetic procedure was developed allowing the synthesis of four new hetero[3]rotaxanes incorporating specific sequences of functional units. Sequence pseudoisomeric rotaxanes which have the naphthalene diimide subunit at two different positions show distinct electrochemical properties. DFT calculations suggest that this differences could arise from a folding of the structure, in which the redox-active moieties stack with a stopper unit. This study presents a blueprint for the construction of hetero [3]rotaxanes with sequential control of the functional units along the track of the axle and paves the way to extend the functionality of mechanically interlocked molecules.

Received 14th October 2021,  
Accepted 25th October 2021

DOI: 10.1039/d1qo01553b

rsc.li/frontiers-organic

## Introduction

Mechanically interlocked molecules (MIMs) have shown great potential as artificial molecular switches and motors performing various tasks at the nanoscopic level and rudimentarily mimicking functions of natural molecules.<sup>1–3</sup> However, the molecular complexity and thereby accessible functions of MIMs are often limited by their symmetrical structures.<sup>4–7</sup> The asymmetrical and directional structure of functional biomolecules derives not only from the centrochirality of their

molecular building blocks originating from a defined structural pool of building blocks, such as DNA nucleotides or amino acids, but also from the specific sequences in which these building blocks are connected. This sequence induces for example the secondary and tertiary structure formation in proteins.<sup>8</sup> The precise positional control of functional units in the natural assembly processes is remarkable. Only minor changes in the sequence can cause a significantly different structure and hence may change function.<sup>9</sup> Therefore, the precise control over the directionality and sequence of sub-components in molecular assemblies is an important goal when constructing functional molecules.

Most MIMs described in the literature are [2]rotaxanes and some examples incorporate directional axles (Fig. 1, top left). Directional axles have been used to build sophisticated molecular machines which operate in a directional fashion. For example, so-called “ribosomal rotaxanes”, incorporate a sequence of amino acids on the track of a directional axle. This amino acid sequence is then sequentially connected to a macrocycle upon chemically induced and directional wheel translation.<sup>10–12</sup>

In a homocircuit[3]rotaxane, two identical macrocycles are threaded onto the axle and a directionality can again only be defined by the axle itself (Fig. 1, top right). Also, oligohomo[n]rotaxanes containing more than two macrocycles have been

<sup>a</sup>Institut für Chemie und Biochemie der Freien Universität Berlin, Arnimallee 20, 14195 Berlin, Germany. E-mail: c.schalley@fu-berlin.de<sup>b</sup>Institut für Chemie und Biochemie der Freien Universität Berlin, Arnimallee 22, 14195 Berlin, Germany<sup>c</sup>Institut für Chemie und Biochemie der Freien Universität Berlin, Fabeckstr. 34/36, 14195 Berlin, Germany

† Electronic supplementary information (ESI) available: Synthetic procedures and characterization data, results from isothermal titration calorimetry, NMR and UV/Vis spectroscopy, tandem mass spectrometry, electrochemical measurements, crystallography and theoretical calculations. CCDC 2047286. For ESI and crystallographic data in CIF or other electronic format see DOI: 10.1039/d1qo01553b

‡ These authors contributed equally to this work.

§ Present address: Department of Chemical and Biological Engineering, Princeton University, Princeton, NJ 08544, USA.



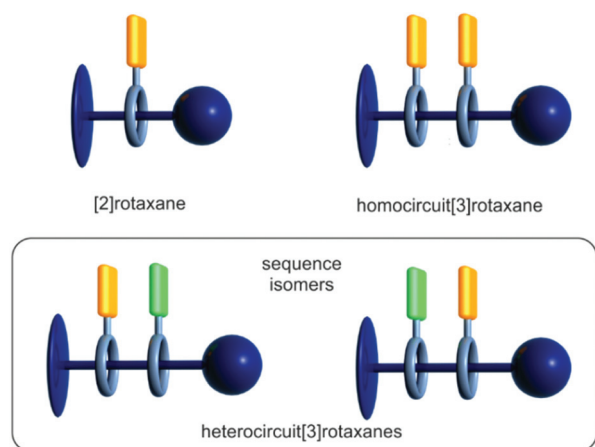


**Fig. 1** Schematic representation of [2] and [3]rotaxanes containing a directional axle (dark blue) and one or two macrocycles (grey) carrying functional units (orange and green).

described.<sup>13–16</sup> In particular, molecular pumps, where multiple macrocycles are threaded onto an axle bringing the system to a higher energy state, are fascinating examples for the application of directional homocircuit[*n*]rotaxanes.<sup>17–19</sup>

If the two threaded macrocycles are not identical, a more complex picture arises. In heterocircuit[3]rotaxanes (Fig. 1, bottom), the directionality is additionally described by the order of macrocycles on the directional axle, consequently, sequence isomers may exist.<sup>20–23</sup> As a consequence of their unique structure, the isomer-specific synthesis of heterocircuit[3]rotaxanes is not trivial.<sup>24</sup> Hence, only few examples of heterocircuitrotaxanes have been described yet.<sup>25</sup> In 1995, the first heterorotaxane synthesis was reported by the group of Stoddart applying a sequential threading approach where a [2]rotaxane is synthesised first. In a second step, the second macrocycle is then threaded onto the axle.<sup>26</sup> A decade passed with minor advancements in this field due to the synthetic obstacles. However, in the last 15 years the interest in heterocircuitrotaxanes increased and outstanding examples could be realised *via* new synthetic approaches.<sup>24,27–34</sup> The group of Loeb, for example, utilised a sequential threading–clipping method yielding a [3]rotaxane facilitating a ring-through-ring molecular shuttling.<sup>35</sup>

Fundamentally different are syntheses using the concept of self-sorting. Here, no sequential addition of components defines the sequences, but instead all components are present in one solution, and find their positions in the final structure through the sorting of orthogonal binding motifs.<sup>36</sup> Even though homorotaxanes or sequence isomers could form, the macrocycles and axles are structurally programmed to prefer one of the heterorotaxane isomers. The group of Goldup, for example, developed a kinetic self-sorting method to obtain heterocircuit[3]rotaxanes.<sup>37</sup> In 2008, the concept of integrative self-sorting was introduced by us for constructing heterorotaxanes using sufficiently different crown/ammonium binding motifs.<sup>38,39</sup> This principle allows to program sequences of two

macrocycles on one axle, for example by descending ring size accompanying binding site selectivity.<sup>36</sup> Later, it was also applied in the synthesis of a [c2]daisy-chain-containing hetero[4]rotaxane<sup>40</sup> and a hetero[6]rotaxane.<sup>41</sup> In a time-dependent mass spectrometric study of the self-sorting process, the crucial role of error correction and kinetic path selection was demonstrated.<sup>42</sup> So far, all examples of heterorotaxanes have a narrow scope of macrocycle combinations and are mostly complex assemblies, but do not contain functional or stimuli-responsive units. The precise arrangement of functional units would pave the way to new molecular switches with emerging properties.

In our recent work on redox-active crown/ammonium complexes we observed that the combination of electron donor tetrathiafulvalene (TTF) and electron acceptor naphthalene diimide (NDI) in a divalent rotaxane yielded a donor–acceptor complex.<sup>43</sup> Furthermore, homooligorotaxanes incorporating TTF-decorated crown ethers enabled the understanding of new switching modes in donor–donor assemblies, such as synchronised pirouetting motion of two macrocycles<sup>44</sup> and an accordion-like motion of the crown ethers.<sup>15</sup> In a study on TTF- and NDI-decorated crown ethers with different cavity sizes, crown [8] ethers revealed a preference for dibenzylammonium and crown[7] wheels for benzyl alkyl ammonium stations, suggesting integrative self-sorting for more functional wheels.<sup>45</sup>

Herein, we propose a blueprint to sequence-sorted heterocircuit[3]rotaxanes using one directional axle and a library of five macrocycles carrying three different types of functional units. This approach allows for unrestricted selection and combination of the functional units in rotaxane structure. We investigate the influence of different ring sizes and binding strengths of the crown ethers involved on the self-sorting equilibrium and heteropseudo[3]rotaxane properties. We apply these findings to the synthesis of four redox-switchable hetero[3]rotaxanes and study the influence of the sequence of functional units on the spectroelectrochemical properties of the rotaxane assemblies.

## Results and discussion

### Design of molecular building blocks

The macrocycle library consists of three types of functionalised crown[8] ethers and two types of functionalised crown[7] ethers (Fig. 2): while **TTFC8** contains an electron-rich pro-aromatic tetrathiafulvalene with electron-donor property (yellow, “donor”), **DBC8** and **BC7** exhibit an aromatic system with no significant donor or acceptor properties (grey, “neutral”), and **NDIC8** and **NDIC7** incorporate an electron-poor aromatic system with electron-acceptor properties (green, “acceptor”). The axle **Ax** contains two secondary ammonium binding stations which are separated by a phenyl group to prevent threading of the crown[7] ethers to the dibenzyl ammonium station (Fig. 2).<sup>38</sup> The directionality of the axle is not only described by the two binding stations, but also, the di-*tert*-



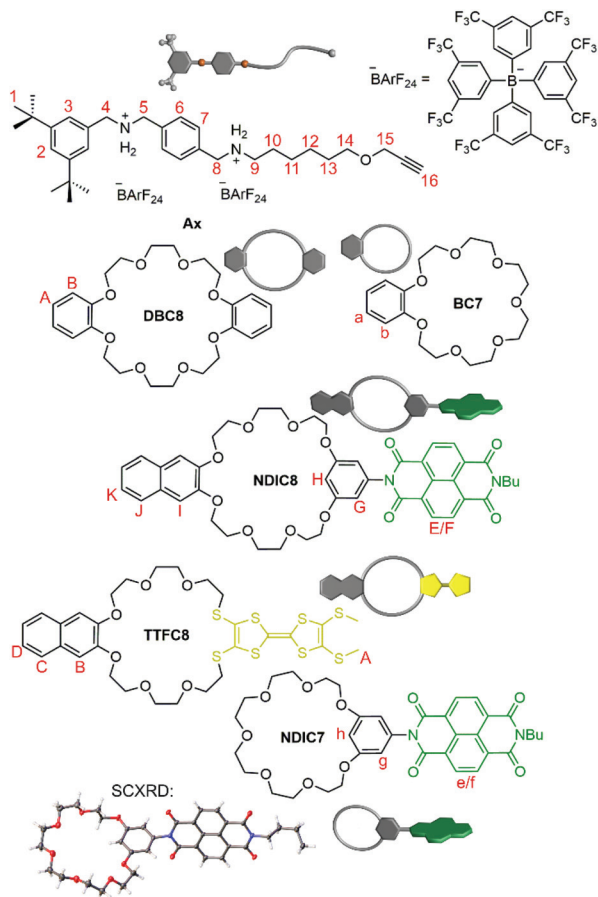


**Fig. 2** Molecular Axle Ax and crown ether macrocycles used in this work. Protons of crown[8] wheels are denoted with capital letters, whereas crown[7] ether protons are denoted with small letters.

butyl stopper. This stopper prevents any wheel threading from this end of the axle and is crucial for programming the wheel sequence. Weakly coordinating tetrakis[3,5-bis(trifluoromethyl)phenyl]borate ( $\text{BARF}_{24}^-$ ) counterions are used to facilitate a stable threaded complex of the weaker binding crown ethers **NDIC8**, **TTFc8** and **NDIC7**. **NDIC7** and axle **Ax** are novel structures and were synthesised along the procedures given in the ESI (ESI section 1<sup>†</sup>). For **NDIC7** we obtained a crystal structure (ESI section 8<sup>†</sup>). In the crystal, the dihedral angle between the phenyl group and the NDI is  $70.01(11)^\circ$ , which is considerably flatter than for **NDIC8**<sup>45</sup> ( $84.18(8)^\circ$ ), in order to facilitate  $\pi$ - $\pi$  interactions between the NDIs of neighbouring **NDIC7** in the solid state. The ring sizes of **NDIC8**, **NDIC7** and **TTFc8** are wider than those of **DBC8** and **BC7**, respectively, as the  $4.766(6)$  Å (**NDIC7**)/ $4.730(4)$  Å (**NDIC8**) distance of the two phenolic O atoms in the NDI-substituted macrocycles as well as the S-S distance of  $3.3136(13)$  Å in **TTFc8**<sup>46</sup> are substantially larger than the O-O distance of  $2.5642(5)$  Å in **DBC8**.<sup>47</sup>

Recently, we have shown that the spectroelectrochemical properties of redox-active crown ethers are not significantly influenced by the crown ether size.<sup>45</sup> This allows us to use the crown ether sizes to program the position of the functional

unit on the axle without changing the spectroelectrochemical properties of the functional units. Therefore, the hetero[3]rotaxane combinations carrying **DBC8/NDIC7** and **NDIC8/BC7** are considered as “sequence pseudoisomers”.

The thermodynamics of pseudorotaxane formation has been studied for monovalent model axles by isothermal titration calorimetry, revealing a 10 times stronger binding for **DBC8** and **BC7** compared to **NDIC8** and **TTFc8**, as well as, **NDIC7**, respectively (for binding data, see ESI Table S1<sup>†</sup>). Crown[8] ethers bind to the aliphatic ammonium slightly weaker than the crown[7] analogues.

### Self-sorting of pseudorotaxanes

The intermediates and products of the self-assembly of equimolar mixtures of divalent axle and the two differently sized generic crown ethers **C8** (pink) and **C7** (blue) are shown schematically in Fig. 3a, where homopseudo[3]rotaxane **PRC8C8** and pseudo[2]rotaxane **PRC7** represent dead-ends on the way to the desired heteropseudo[3]rotaxane **PRC8C7**. Error-correction is necessary to overcome these dead-ends.

For all six combinations of one **C8**, one **C7** and **Ax**, equimolar solutions were equilibrated for 16 days at room temperature after which no further change in the NMR spectra was observed. Although a full assignment of all signals in the highly complex  $^1\text{H}$  NMR spectra is not straightforward due to severe signal overlap (ESI section 3<sup>†</sup>), the four methylene signals (H(4), H(5), H(8) and H(9)) can be identified in the COSY spectra and are highly indicative for pseudorotaxane formation (Fig. 3b and e and ESI section 3<sup>†</sup>). For the mixture containing **TTFc8**, **BC7** and **Ax**, three major species could be identified and assigned by the chemical shift of their methylene protons to the heteropseudo[3]rotaxane **PRTTFC8BC7** (Fig. 3b, blue), homopseudo[3]rotaxane **PRTTFC8TTFc8** (Fig. 3b, red) and pseudo[2]rotaxane **PRBC7** (Fig. 3b, green). Changing the smaller macrocycle to the weaker binding **NDIC7** a higher amount of heteropseudo[3]rotaxane **PRTTFC8NDIC7** (Fig. 3e, blue) is observed. While the pseudo[2]rotaxane **PRNDIC7** cannot be identified, a small fraction of pseudo[2]rotaxane **PRTTFC8** (Fig. 3e, brown) is visible. The other four combinations show similar results (ESI section 3<sup>†</sup>). As calculated from the integrals of the methylene protons H(4) and H(5), the heteropseudo[3]rotaxanes are preferentially formed with amounts of 56–74% in all six cases (Table 1). For a non-self-sorting system with a directional axle a statistical amount for one specific heteropseudo[3]rotaxane of 25% would be expected. The weaker binding macrocycle **NDIC7** forms the corresponding heteropseudo[3]rotaxanes with higher selectivity as compared to **BC7**.

Due to the charge inherent in all pseudorotaxanes under study, electrospray ionisation mass spectrometry (ESI-MS) is a valuable additional analytical technique to study the self-sorting equilibrium (Fig. 3c and f and ESI section 4<sup>†</sup>). Due to differences in ionisation efficiencies, the overall abundances cannot be directly related to solution concentrations, yet a semiquantitative overview of the formation of the pseudorotaxanes with reaction time can certainly be obtained. A solution



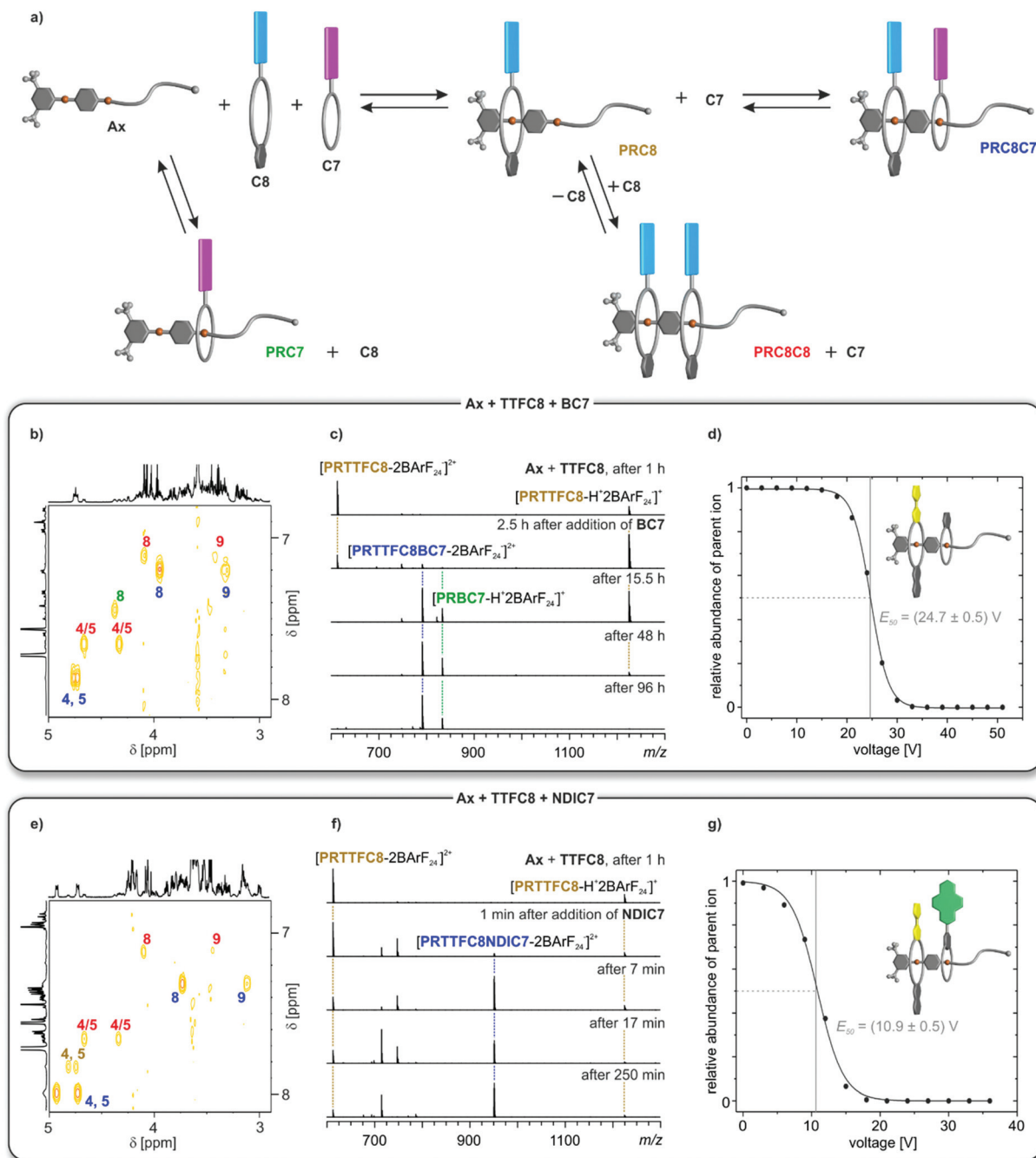


**Fig. 3** (a) Schematic representation of the self-sorting equilibrium for two generic crown ethers **C8** (pink) and **C7** (blue). Spectra in (b, c and d) use an equimolar solution of **TTFC8**, **BC7** and **Ax**; and in (e, f and g) of **TTFC8**, **NDIC7** and **Ax**. Signals of protons or ions for the heteropseudo[3]rotaxanes are labeled in blue, for the homopseudo[3]rotaxanes in red, for the pseudo[2]rotaxane **PRTTFC8** in brown and to the crown[7] pseudo[2]rotaxanes in green. (b and e) Partial  $^1\text{H}, ^1\text{H}$  COSY spectra (700 MHz,  $\text{CD}_2\text{Cl}_2$ , 298 K, 5 mM, 16 d). For full  $^1\text{H}$  NMR spectra and integration see Fig. S24 and S26.† (c and f) Time-dependent ESI-MS spectra in  $\text{CH}_2\text{Cl}_2$  at 293 K. Non-labeled peaks correspond to different crown ether ions (ESI section 4†). (d and g) Survival yield curves obtained for mass-selected ions of **PRTTFC8BC7**  $m/z$  791 (d) and **PRNDIC8BC7**  $m/z$  951 (g) obtained from CID experiments at increasing collision voltages. Solid lines represent a sigmoidal fitting to determine 50% survival yield voltages  $E_{50}$  (Table 1 and ESI section 4†).

of **Ax** and **TTFC8** was equilibrated for 1 h. In the ESI mass spectrum, pseudo[2]rotaxane **PRTTFC8** can be observed in the two +1 and +2 charge states (Fig. 3c). The homopseudo[3]rotaxane **PRTTFC8TTFC8** is not observed in the mass spectrum, as it forms **PRTTFC8** rapidly upon dilution and ionisation due to

the low thermodynamic and kinetic stability of **PRTTFC8TTFC8**. After addition of **BC7**, heteropseudo[3]rotaxane **PRTTFC8BC7** forms only slowly on an hour time scale, as the threading of **BC7** is a slow process. At the same time, also the dead-end pseudo[2]rotaxane **PRBC7** is formed.





**Table 1** Characterisation parameters for the self-sorting equilibrium of six macrocycle combinations with axle **Ax** in equimolar solutions obtained by  $^1\text{H}$  NMR spectroscopy, time-dependent and tandem mass spectrometry (for full data set and experimental details see ESI sections 3 and 4†)

Macrocycle combination	DBC8 BC7	TTFC8 BC7	NDIC8 BC7	DBC8 NDIC7	TTFC8 NDIC7	NDIC8 NDIC7
Hetero[3]pseudorotaxane amount <sup>a</sup>	58%	56%	57%	72%	70%	74%
Threading timeframe <sup>b</sup>	Days	Days	Days	Hours	Hours	Hours
$E_{50}$ <sup>c</sup>	21.7 V	24.7 V	27.1 V	9.4 V	10.9 V	11.4 V

<sup>a</sup> Calculated from signal integration in  $^1\text{H}$  NMR experiments (700 MHz,  $\text{CD}_2\text{Cl}_2$ , 298 K, 5 mM, 16 d). Amounts are given as percentages of all identified pseudorotaxane species (estimated error: 5%). <sup>b</sup> Qualitative estimation from time-dependent ESI-MS, when 90% of the maximum heteropseudo[3]rotaxane concentration is reached. <sup>c</sup> Estimated error amounts to 0.5 V.

In marked contrast, hetero[3]pseudorotaxane **PRTTFC8NDIC7** forms already within minutes upon addition of the wider **NDIC7** to the solution of **Ax** and **TTFC8**. After 4 h virtually no changes are observed in the spectrum (Fig. 3f). The same experiments with the other crown[8] ethers revealed that the equilibrium for **NDIC7**-containing mixtures are reached after a couple of hours, while mixtures including **BC7** take several days to equilibrate (Table 1 row 3 and ESI section 4†). This difference can be rationalised by the bigger ring size and thereby faster threading kinetics of **NDIC7**. Slower threading kinetics come together with a slower error correction process, as it can also be seen by the appearance of dead-end **PRBC7** in the mass spectrum as well as the  $^1\text{H}$  NMR experiments. The different crown[8] ethers do not significantly alter the overall threading kinetics and heteropseudo[3]rotaxane **PRC8C7** selectivity, as their threading is comparably fast.<sup>42</sup>

Collision-induced dissociation (CID) experiments with mass-selected heteropseudo[3]rotaxane ions were used to establish the sequence of the pseudorotaxanes and to exclude non-threaded binding (ESI section 4†). For all heteropseudo[3]rotaxanes incorporating **NDIC7**, the CID mass spectra showed the loss of the crown[7] ether as the first fragmentation step (ESI Fig. S39–S41†). In contrast, **BC7** containing heteropseudo[3]rotaxane ions fragment by breaking of a covalent bond first (ESI Fig. S36–S38†). The 50% survival yield voltages  $E_{50}$  obtained from the CID mass spectra allow to compare the gas-phase stabilities of the heteropseudo[3]rotaxane assemblies (Fig. 3d and g, Table 1 and ESI Fig. S42†). **PRTTFC8BC7** exhibits a significantly higher gas phase stability as compared to **PRTTFC8NDIC7** (Fig. 3d and g). Also,  $E_{50}$  mainly is impacted by the threaded crown[7] ether (Table 1 row 4). Taking into account, that the isolated ions are doubly charged, the  $E_{1/2}$  values of all six heteropseudo[3]rotaxane ions are significantly higher than for a non-threaded crown/*sec*-ammonium complex.<sup>46</sup> Overall, these observations evidence the desired sequence and threaded structures were achieved in all six heteropseudo[3]rotaxane combinations.

These results clearly show that the second, smaller macrocycles **NDIC7** and **BC7** dominate the thermodynamic and kinetic properties of the self-sorting equilibrium. The benefit of faster threading kinetics for a self-sorting process can be highlighted by the observation of a higher selectivity for the **NDIC7** containing heteropseudo[3]rotaxanes. The higher binding constants achieved by using  $\text{BARF}_{24}^-$  counterions com-

pared to previous studies<sup>38,39,42</sup> where  $\text{PF}_6^-$  counterions were used, caused a higher kinetic barrier for the dethreading reaction of **BC7**, which is the crucial step for all error-correction processes, resulting in a comparably long equilibration time. Yet, the used conditions are robust and facilitate the formation of heteropseudo[3]rotaxanes for all combinations.

### A cascade-stoppered pseudo[3]rotaxane

The slow self-sorting process together with the remarkably high gas phase stability of **BC7**-containing heteropseudo[3]rotaxanes motivated us to study **PRTTFC8BC7** in a greater detail. Although a few exceptions are known,<sup>34,46</sup> crown/ammonium pseudorotaxanes are usually not sufficiently stable to survive column chromatography. Therefore, it is surprising that the pseudorotaxane **PRTTFC8BC7** was chromatographically isolated in 24% yield. For all other combinations of wheels under study here, the formed complexes dissociate on the silica column. Pseudo[3]rotaxanes with **NDIC7** dissociated quickly. The two other **BC7**-containing pseudo[3]rotaxanes required more polar mobile phases, which undermine their stability so that they also dissociate during chromatography. The stronger binding wheel **BC7** on the outer binding site acts as a stopper for the weaker binding wheel **TTFC8** on the dibenzyl ammonium binding site. Pseudo[3]rotaxanes of two **TTFC8** on **Ax** could not be isolated as they fell apart during the purification. This underlines the exceptional importance of the sequence in which the macrocycles are threaded on the one-side stoppered axle for the physico-chemical properties of the assembly.

For comparison, the rotaxane **RTTFC8BC7** was synthesised in 15% yield by adding 1.5 equiv. of 2,6-dimethoxybenzotrile oxide stopper **St1** and stirring for one day at 35 °C. Fig. 4 shows the  $^1\text{H}$  NMR shifts of (**P**)**RTTFC8BC7** in comparison to the axle **Ax**. Characteristic shifts include benzylic methylene protons H(4/5) and H(9), which shift downfield ( $\Delta\delta \geq +0.4$  ppm and +0.2 ppm) upon threading of **TTFC8** and **BC7**. Additionally, methylene protons H(8) shift upfield by 0.3 ppm. Both is true for the pseudo[3]rotaxane **PRTTFC8BC7** and the [3]rotaxane **RTTFC8BC7**. A strong downfield shift by 3.9 ppm of the former alkyne proton H(16) is observed, as it is incorporated into the newly formed isoxazole moiety. The methylene group H(15) adjacent to the former alkyne also shifts by 0.4 ppm downfield. Except for the protons on stopper **St1** and H(15,16), the shifts of pseudorotaxane **PRTTFC8BC7** and rotaxane **RTTFC8BC7** are similar.



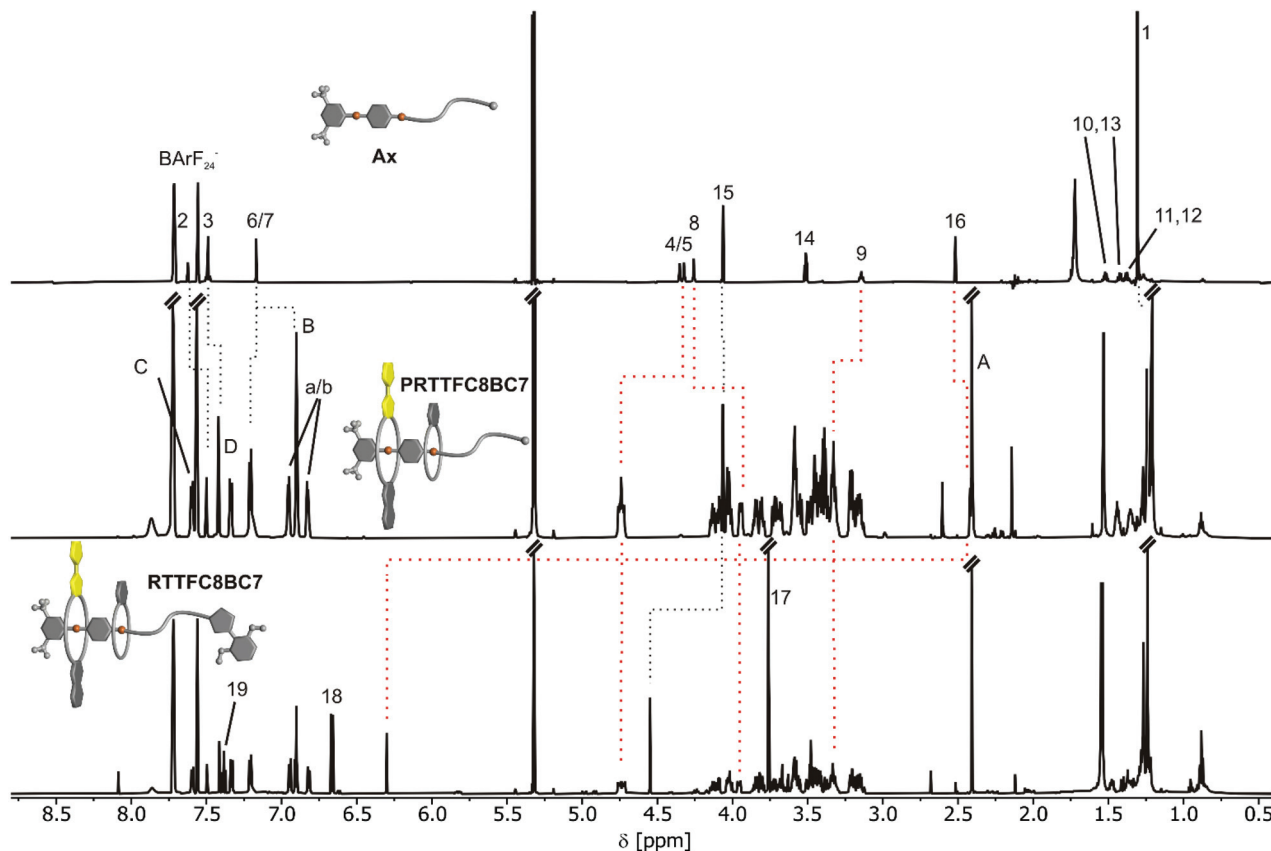


Fig. 4  $^1\text{H}$  NMR comparison of free axle Ax, PRTTFC8BC7 and RTTFC8BC7. Characteristic shifts are highlighted by red dotted lines (ESI section 1.4† for full signal assignment).

To test the stability in a more polar solvent, chromatographically isolated PRTTFC8BC7 was dissolved in acetonitrile in high dilution (1  $\mu\text{M}$ ). After 6 h a significant amount of threaded PRTTFC8BC7 could still be observed by ESI-MS (ESI Fig. S43†). It took multiple days to reach thermodynamic equilibrium in which virtually no complex has survived, evidencing the high kinetic stability and nearly rotaxane-like behaviour of PRTTFC8BC7.

Electrochemical characterisation of both species (P) RTTFC8BC7, by cyclic voltammetry (CV) and differential pulse voltammetry (DPV) show similar results (Fig. 5). The two reversible oxidations of TTF are anodically shifted, as expected for wheel TTFc8 bound to an ammonium site.<sup>48</sup> In previous work, we reported that the ammonium site is expelled upon oxidation due to coulombic repulsion with the oxidised TTF unit. Electrochemically induced dethreading results in a new signal for the TTF<sup>+/2+</sup> redox couple of unbound TTFc8 at  $\sim 1$  V against decamethylferrocene/decamethylferrocenium ( $\text{Fc}^{0/+}$ ).<sup>48</sup> Sterically demanding end groups can kinetically hamper oxidation-induced dethreading efficiently.<sup>46</sup> However, for both, pseudorotaxane and rotaxane, no dethreading is observed and redox potentials vary only marginally. This underlines the remarkable stability, which is exceptional for a non-interlocked crown/ammonium complex, and rotaxane-like behaviour of PRTTFC8BC7 as already observed in the CID

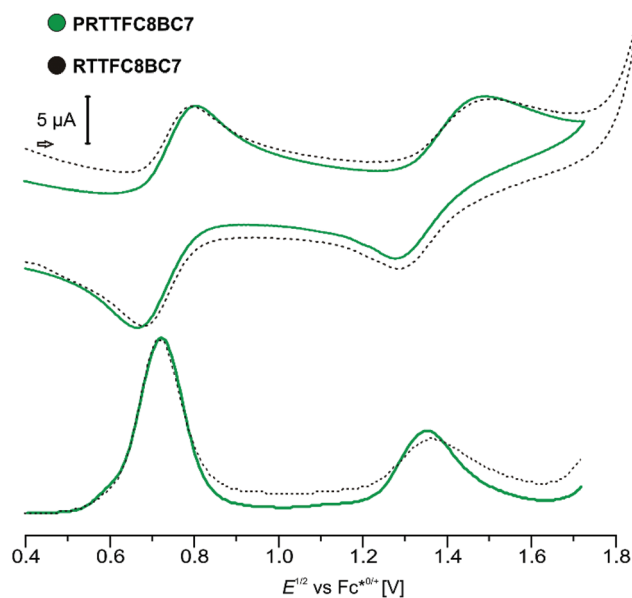


Fig. 5 CV and DPV of (pseudo)hetero[3]rotaxanes (P)RTTFC8BC7 (1,2-dichloroethane with  $n\text{-Bu}_4\text{NBARF}_{24}$  as the electrolyte (0.1 M) 1.5 mM analyte,  $25\text{ mV s}^{-1}$  scan rate for CV and 225 mV modulation amplitude, 50 ms modulation time, 5 mV step potential and 0.5 s interval time for DPV).



measurements. The increased TTF oxidation potentials (+126 and 362 mV for first and second oxidation) together with its inability to dethread turn **PRTTFC8BC7** into an electrochemically “frustrated” pseudorotaxane that is kinetically trapped in a metastable state.

### Hetero[3]rotaxane synthesis

The self-sorting experiments show pseudohetero[3]rotaxane formation to be prominent for all C8/C7 macrocycle combinations. We therefore developed a generally applicable synthetic procedure for the synthesis of the corresponding hetero[3]rotaxanes, which does not depend on a prior chromatographic purification of the pseudo[3]rotaxane precursors. The pseudorotaxane mixtures were treated with the 2,6-dimethoxybenzonitrile stopper **St1**. This reaction was optimised by using up to six equivalents of the smaller macrocycle relative to the axle to reduce homo[3]rotaxane formation (for detailed synthetic procedures and characterisation data see ESI section 1.4†). Afterwards, the excess of the smaller macrocycle was recycled. Fig. 6 shows the isolated hetero[3]rotaxanes which all feature the diagnostic  $^1\text{H}$  NMR shifts upon threading and rotaxanation as well as the diastereotopic splitting of the crown ether methylene groups as described in the previous chapter (ESI Fig. S14, S17 and S20†). The desired macrocycle sequence and the mechanically interlocked structure of the

four hetero[3]rotaxanes was confirmed by CID experiments with mass-selected hetero[3]rotaxane ions, where at very high collision energies axle cleavage is observed as the major fragmentation pathway (ESI Fig. S49–S52†). The isolated examples consist of a “donor-neutral” (yellow-grey), “donor-acceptor” (yellow-green) and the pseudo sequence isomers “acceptor-neutral” (green-grey) and “neutral-acceptor” (grey-green) hetero[3]rotaxanes. The isolated yields compare very well to the majority of isolated heterorotaxanes in the literature.<sup>26,28,35,37</sup> Additionally, the isolation of hetero[3]rotaxanes with different wheel combinations without self-sorting would certainly be a very tedious process.

### Optoelectronic properties of sequence-sorted rotaxanes

A comparison between isolated hetero[3]rotaxanes and the free macrocycles **TTFC8**, **NDIC7** or **NDIC8** allow an assessment of the influence of the macrocycle sequence on the electrochemical properties. Fig. 7 summarises all peak potentials obtained by DPV measurements in 1,2-dichloroethane with *n*-Bu<sub>4</sub>NBArF<sub>24</sub> as supporting electrolyte (ESI Table S2†). The potentials are referenced against the Fc<sup>0/+</sup> redox-couple. The peaks at positive potentials can be attributed to the two reversible redox waves, TTF<sup>(0/+)</sup> and TTF<sup>(+/2+)</sup>. As previously shown,<sup>48</sup> all species with **TTFC8** bound to an axle are shifted anodically in a comparable fashion. The second macrocycle

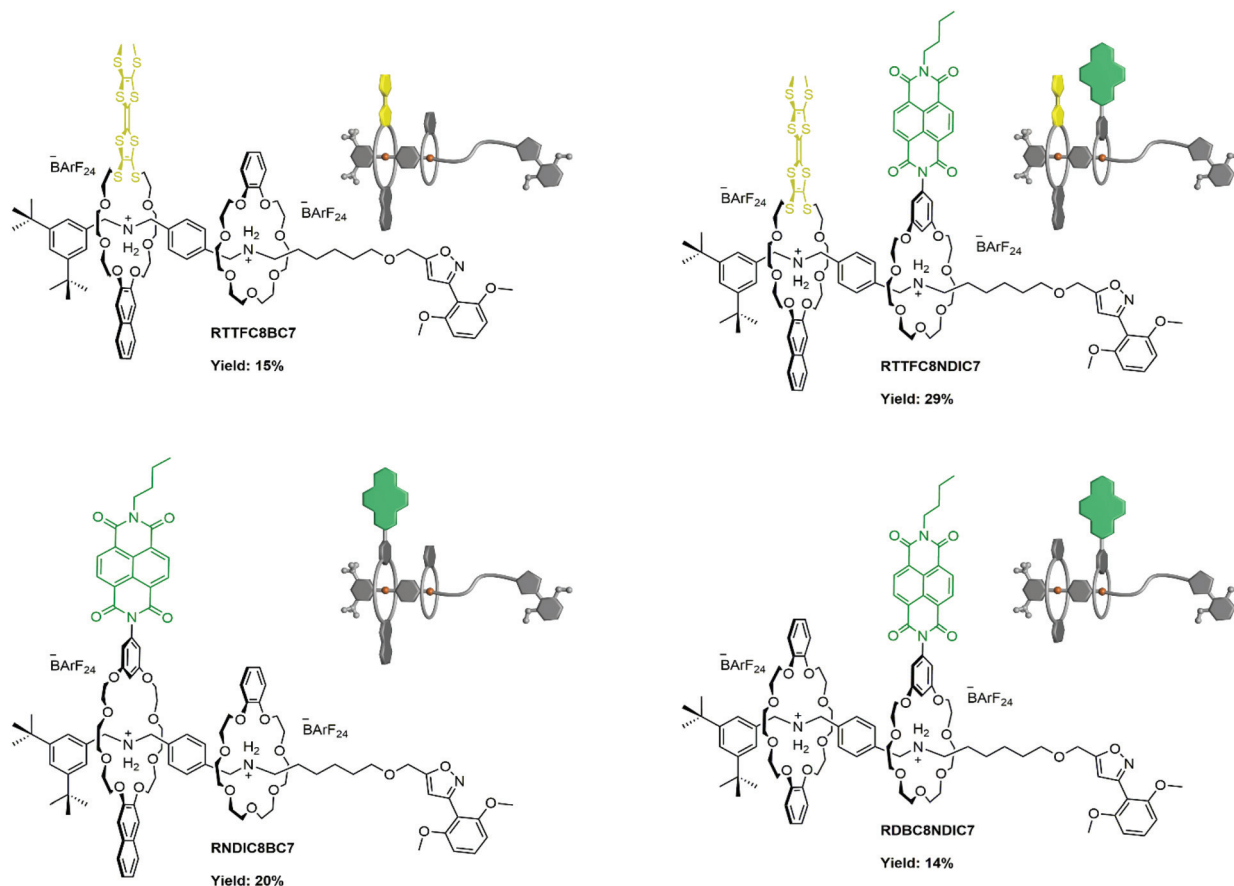


Fig. 6 Hetero[3]rotaxanes synthesised from the pseudorotaxane mixtures and their isolated yields.



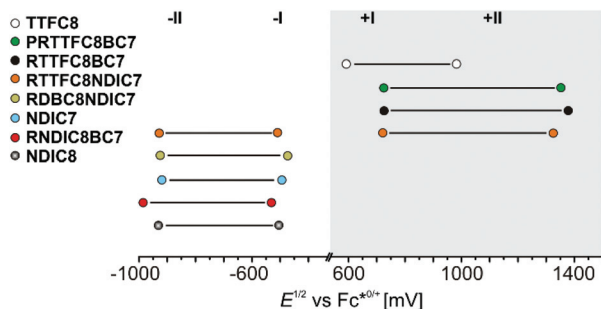


Fig. 7 Correlation diagram of half-wave potentials for hetero[3]rotaxanes and free macrocycles determined by DPV (Table S2,† the error is estimated to be  $\pm 10$  mV).

does not have strong impact on the oxidation of **TTFC8** in the rotaxane as can be seen on the similar oxidation potentials of donor–acceptor rotaxane **RTTFC8NDIC7** and donor-neutral rotaxane **RTTFC8BC7**.

In contrast, the peaks at negative potentials are the two reversible reductions  $\text{NDI}^{(0/+)}$  and  $\text{NDI}^{(+/-)}$ . For the free wheels **NDIC7** and **NDIC8** both reduction peaks are similar ( $\Delta E^{1/2} = 11$  mV for  $\text{NDI}^{(0/+)}$  and  $\Delta E^{1/2} = 16$  mV for  $\text{NDI}^{(+/-)}$ ), as expected from their similar structures. For [3]rotaxane **RNDIC8BC7** a significant cathodic shift of 20 mV for  $\text{NDI}^{(0/+)}$  and 55 mV for  $\text{NDI}^{(+/-)}$  compared to wheel **NDIC8** is observed. In contrast, [3]rotaxanes **RTTFC8NDIC7** and **RDBC8NDIC7** only show minor differences in the reduction potentials ( $\Delta E^{1/2} \leq 10$  mV for  $\text{NDI}^{(0/+)}$  and  $\Delta E^{1/2} \leq 11$  mV for  $\text{NDI}^{(+/-)}$ ) compared to wheel **NDIC7**. Consequently, the position of the NDI-unit on the axle indeed has a significant impact on the electrochemical properties. For **NDIC7** we could not determine a significant influence of the second larger macrocycle neither being neutral nor electron donor. The difference of electrochemical properties of the NDI sequence pseudoisomers **RNDIC8BC7** and **RDBC8NDIC7** presumably occurs as a consequence of the sequence rather than the macrocycle combination. Indeed, DFT calculations and conformational analysis at the PBEh-3c level<sup>49</sup> using the COSMO<sup>50</sup> solvation model provide a molecular structure for **RNDIC8BC7**, where the NDI-unit stacks with the dimethoxybenzene stopper (Fig. 8a and ESI section 7†).

For donor–acceptor hetero[3]rotaxane **RTTFC8NDIC7** the calculated structure displays a stacked conformation of TTF- and NDI-unit as well as the dimethoxybenzene stopper (Fig. 8b and ESI section 7†). Even though it is rather difficult to understand the exact reason for the different potential shifts of the NDI-unit, the distance of NDI-bearing crown ether to the stopper unit seems to have an influence. Yet, spin-density plots are TTF-localised for the oxidised species and NDI-localised for the reduced species (ESI Fig. S60 and S61†). Chemical oxidation of **RTTFC8NDIC7** shows similar bands in the UV/Vis spectra as those of the free wheel **TTFC8** for the three redox states of TTF (ESI section 6†). Together with the electrochemical data, these observations demonstrate the spectroelectric properties of **TTFC8** to be retained within the mechanically interlocked assembly.

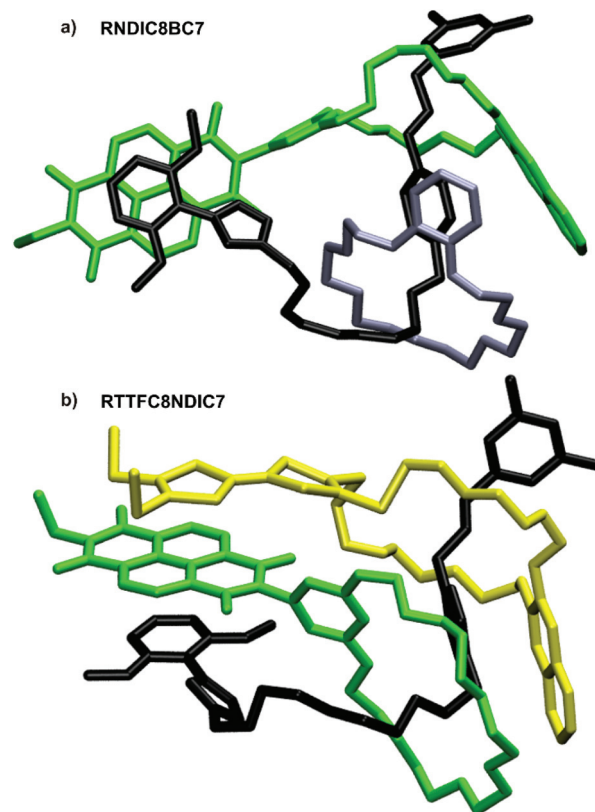


Fig. 8 Calculated structures of (a) **RNDIC8BC7** and (b) **RTTFC8NDIC7**, with the axle denoted in black, **TTFC8** in yellow, **BC7** in grey and **NDIC7** as well as **NDIC8** in green.

## Conclusions

We demonstrated how integrative self-sorting can be applied as a molecular programming language to dictate the sequence of redox-switchable units along a molecular track. For the first time, we integrated functional redox-switchable units, namely TTF and NDI, into hetero[3]rotaxanes using this strategy.

The properties of the self-sorting process are dominated by the second macrocycle in the sequence. While the wider and weaker binding **NDIC7** facilitates fast threading kinetics, as well as good hetero[3]rotaxane selectivity, the smaller and stronger binding **BC7** results in slow threading kinetics and a slow error correction as well as in lower selectivities for the heteropseudo[3]rotaxane. The **BC7**-containing heteropseudo[3]rotaxanes show a surprising stability. The pseudorotaxane **PRITFC8BC7**, could even be isolated by chromatography and thus shows rotaxane-like behaviour with **BC7** being a pseudostopper. Upon TTF oxidation, an electrochemically “frustrated” pseudorotaxane forms, in which the larger wheel experiences charge repulsion with the axle ammonium station, but is unable to dethread.

With the synthesis of four new hetero[3]rotaxanes, we demonstrate that different functional units can be placed in different sequences on the axle, as long as one crown[8] ether and one crown[7] ether is used. While for each individual





hetero[3]rotaxane combination more selective conditions such as counterion, solvent or equilibration time, can be found, our synthetic approach is general and robust and facilitates the synthesis of hetero[3]rotaxanes with varying crown ether sizes, binding strength and functional units. This concept is applicable to other functionalised crown ethers. By the ease to decorate crown ethers<sup>51</sup> with various functional moieties, our approach represents a modular strategy to incorporate and combine a broad variety of such units using hetero[3]rotaxanes as the scaffold.

In our work the functional units were combined to generate a donor-neutral (RTTFC8BC7), a donor-acceptor (RTTFC8NDIC7), an acceptor-neutral (RNDIC8BC7) and a neutral-acceptor (RD8C8NDIC7) rotaxane. Studying the electrochemical properties of these assemblies, we could show that the donor moiety (TTF) was marginally influenced. Instead, the acceptor moiety (NDI) showed shifted redox potentials depending on the position on the axle, probably depending on the availability of interactions to one of the stoppers. Regardless of their sequence, the redox-active units retain their reversible spectroelectrochemical properties upon incorporation into the mechanically interlocked structure. Using these results, highly directional functional molecules bearing different macrocycles can be envisioned and facilitate new switching modes or functions for rotaxane assemblies.

## Author contributions

The project was developed by H. H. and M.G. H. H., M. G. and C. A. S. wrote the manuscript with main contributions from H. H. and M. G. The synthetic work was carried out by M. G., C. D., S. M. R., L. F. and H. H. with main contributions coming from M. G. H. H. conducted and evaluated all time dependent NMR and tandem MS experiments. M. G. performed further NMR, UV/Vis and CV/DPV experiments and prepared the single crystals. H. V. S. helped with data evaluation and conception. H. H. measured and analysed the ITC data. All computational work was done by F. W. and B. P. S. M. R. and M. M. measured and solved the SCXRD data. Both M. G. and H. H. contributed equally and have the right to list their name first in their CV. All Authors contributed to the final version of the manuscript.

## Conflicts of interest

There are no conflicts to declare.

## Acknowledgements

We thank Sebastian Müller for help with the synthesis. We are grateful for funding from the Deutsche Forschungsgemeinschaft (DFG; project number 434455294) and acknowledge the assistance of the Core Facility BioSupraMol supported by the DFG. Furthermore, F. W. and

B. P. acknowledge the DFG for funding (PA 1360/16-1) and the North-German Supercomputing Alliance (Norddeutscher Verbund für Hoch- und Höchstleistungsrechnen) for providing computational resources.

## Notes and references

- 1 S. Erbas-Cakmak, D. A. Leigh, C. T. McTernan and A. L. Nussbaumer, Artificial Molecular Machines, *Chem. Rev.*, 2015, **115**, 10081–10206.
- 2 Y. Feng, M. Ovalle, J. S. W. Seale, C. K. Lee, D. J. Kim, R. D. Astumian and J. F. Stoddart, Molecular Pumps and Motors, *J. Am. Chem. Soc.*, 2021, **143**, 5569–5591.
- 3 L. Zhang, V. Marcos and D. A. Leigh, Molecular machines with bio-inspired mechanisms, *Proc. Natl. Acad. Sci. U. S. A.*, 2018, **115**, 9397–9404.
- 4 A. Coskun, M. Banaszak, R. D. Astumian, J. F. Stoddart and B. A. Grzybowski, Great expectations: can artificial molecular machines deliver on their promise?, *Chem. Soc. Rev.*, 2012, **41**, 19–30.
- 5 M. Xue, Y. Yang, X. Chi, X. Yan and F. Huang, Development of Pseudorotaxanes and Rotaxanes: From Synthesis to Stimuli-Responsive Motions to Applications, *Chem. Rev.*, 2015, **115**, 7398–7501.
- 6 M. Baroncini, L. Casimiro, C. de Vet, J. Groppi, S. Silvi and A. Credi, Making and Operating Molecular Machines: A Multidisciplinary Challenge, *ChemistryOpen*, 2018, **7**, 169–179.
- 7 C. A. Schalley, K. Beizai and F. Vögtle, On the Way to Rotaxane-Based Molecular Motors: Studies in Molecular Mobility and Topological Chirality, *Acc. Chem. Res.*, 2001, **34**, 465–476.
- 8 N. Badi and J. F. Lutz, Sequence control in polymer synthesis, *Chem. Soc. Rev.*, 2009, **38**, 3383–3390.
- 9 M. Kosloff and R. Kolodny, Sequence-similar, structure-dissimilar protein pairs in the PDB, *Proteins*, 2008, **71**, 891–902.
- 10 B. Lewandowski, G. De Bo, J. W. Ward, M. Pappmeyer, S. Kuschel, M. J. Aldegunde, P. M. Gramlich, D. Heckmann, S. M. Goldup, D. M. D'Souza, A. E. Fernandes and D. A. Leigh, Sequence-specific peptide synthesis by an artificial small-molecule machine, *Science*, 2013, **339**, 189–193.
- 11 G. De Bo, S. Kuschel, D. A. Leigh, B. Lewandowski, M. Pappmeyer and J. W. Ward, Efficient assembly of threaded molecular machines for sequence-specific synthesis, *J. Am. Chem. Soc.*, 2014, **136**, 5811–5814.
- 12 C. M. Wilson, A. Gualandi and P. G. Cozzi, A rotaxane turing machine for peptides, *ChemBioChem*, 2013, **14**, 1185–1187.
- 13 A. J. Avestro, D. M. Gardner, N. A. Vermeulen, E. A. Wilson, S. T. Schneebeli, A. C. Whalley, M. E. Belowich, R. Carmieli, M. R. Wasielewski and J. F. Stoddart, Gated electron sharing within dynamic naphthalene diimide-based oligorotaxanes, *Angew. Chem., Int. Ed.*, 2014, **53**, 4442–4449.



- 14 D. Sluysmans, S. Hubert, C. J. Bruns, Z. Zhu, J. F. Stoddart and A. S. Duwez, Synthetic oligorotaxanes exert high forces when folding under mechanical load, *Nat. Nanotechnol.*, 2018, **13**, 209–213.
- 15 H. V. Schröder, F. Stein, J. M. Wollschläger, S. Sobottka, M. Gaedke, B. Sarkar and C. A. Schalley, Accordion-Like Motion in Electrochemically Switchable Crown Ether/Ammonium Oligorotaxanes, *Angew. Chem., Int. Ed.*, 2019, **58**, 3496–3500.
- 16 H. Y. Zhou, Q. S. Zong, Y. Han and C. F. Chen, Recent advances in higher order rotaxane architectures, *Chem. Commun.*, 2020, **56**, 9916–9936.
- 17 C. Cheng, P. R. McGonigal, S. T. Schneebeli, H. Li, N. A. Vermeulen, C. Ke and J. F. Stoddart, An artificial molecular pump, *Nat. Nanotechnol.*, 2015, **10**, 547–553.
- 18 C. Pezzato, M. T. Nguyen, D. J. Kim, O. Anamimoghadam, L. Mosca and J. F. Stoddart, Controlling Dual Molecular Pumps Electrochemically, *Angew. Chem., Int. Ed.*, 2018, **57**, 9325–9329.
- 19 S. Amano, S. D. P. Fielden and D. A. Leigh, A catalysis-driven artificial molecular pump, *Nature*, 2021, **594**, 529–534.
- 20 H. Y. Au-Yeung and A. W. H. Ng, Mechanical Interlocking of Macrocycles in Different Sequences, *Synlett*, 2020, **31**, 309–314.
- 21 A. M. Fuller, D. A. Leigh and P. J. Lusby, Sequence isomerism in [3]rotaxanes, *J. Am. Chem. Soc.*, 2010, **132**, 4954–4959.
- 22 E. A. Neal and S. M. Goldup, Chemical consequences of mechanical bonding in catenanes and rotaxanes: isomerism, modification, catalysis and molecular machines for synthesis, *Chem. Commun.*, 2014, **50**, 5128–5142.
- 23 C. Talotta, C. Gaeta, Z. Qi, C. A. Schalley and P. Neri, Pseudorotaxanes with self-sorted sequence and stereochemical orientation, *Angew. Chem., Int. Ed.*, 2013, **52**, 7437–7441.
- 24 E. A. Wilson, N. A. Vermeulen, P. R. McGonigal, A. J. Avestro, A. A. Sarjeant, C. L. Stern and J. F. Stoddart, Formation of a hetero[3]rotaxane by a dynamic component-swapping strategy, *Chem. Commun.*, 2014, **50**, 9665–9668.
- 25 X. Q. Wang, W. J. Li, W. Wang and H. B. Yang, Heterorotaxanes, *Chem. Commun.*, 2018, **54**, 13303–13318.
- 26 D. B. Amabilino, P. R. Ashton, M. Bělohradský, F. M. Raymo and J. F. Stoddart, The controlled self-assembly of a [3]rotaxane incorporating three constitutionally different components, *J. Chem. Soc., Chem. Commun.*, 1995, **7**, 747–750.
- 27 J. E. Lewis, J. Winn, L. Cera and S. M. Goldup, Iterative Synthesis of Oligo[n]rotaxanes in Excellent Yield, *J. Am. Chem. Soc.*, 2016, **138**, 16329–16336.
- 28 X. Zhao, X. K. Jiang, M. Shi, Y. H. Yu, W. Xia and Z. T. Li, Self-assembly of novel [3]- and [2]rotaxanes with two different ring components: donor-acceptor and hydrogen bonding interactions and molecular-shuttling behavior, *J. Org. Chem.*, 2001, **66**, 7035–7043.
- 29 A. Joosten, Y. Trolez, V. Heitz and J. P. Sauvage, Use of cleavable coordinating rings as protective groups in the synthesis of a rotaxane with an axis that incorporates more chelating groups than threaded macrocycles, *Chem. – Eur. J.*, 2013, **19**, 12815–12823.
- 30 X. Hou, C. Ke and J. F. Stoddart, Cooperative capture synthesis: yet another playground for copper-free click chemistry, *Chem. Soc. Rev.*, 2016, **45**, 3766–3780.
- 31 C. Ke, R. A. Smaldone, T. Kikuchi, H. Li, A. P. Davis and J. F. Stoddart, Quantitative emergence of hetero[4]rotaxanes by template-directed click chemistry, *Angew. Chem., Int. Ed.*, 2013, **52**, 381–387.
- 32 C. Ke, N. L. Strutt, H. Li, X. Hou, K. J. Hartlieb, P. R. McGonigal, Z. Ma, J. Iehl, C. L. Stern, C. Cheng, Z. Zhu, N. A. Vermeulen, T. J. Meade, Y. Y. Botros and J. F. Stoddart, Pillar[5]arene as a co-factor in templating rotaxane formation, *J. Am. Chem. Soc.*, 2013, **135**, 17019–17030.
- 33 X. Hou, C. Ke, C. J. Bruns, P. R. McGonigal, R. B. Pettman and J. F. Stoddart, Tunable solid-state fluorescent materials for supramolecular encryption, *Nat. Commun.*, 2015, **6**, 6884.
- 34 M. A. Soto, F. Lelj and M. J. MacLachlan, Programming permanent and transient molecular protection via mechanical stoppering, *Chem. Sci.*, 2019, **10**, 10422–10427.
- 35 K. Zhu, G. Baggi and S. J. Loeb, Ring-through-ring molecular shuttling in a saturated [3]rotaxane, *Nat. Chem.*, 2018, **10**, 625–630.
- 36 Z. He, W. Jiang and C. A. Schalley, Integrative self-sorting: a versatile strategy for the construction of complex supramolecular architecture, *Chem. Soc. Rev.*, 2015, **44**, 779–789.
- 37 E. A. Neal and S. M. Goldup, A Kinetic Self-Sorting Approach to Heterocircuit [3]Rotaxanes, *Angew. Chem., Int. Ed.*, 2016, **55**, 12488–12493.
- 38 W. Jiang, H. D. Winkler and C. A. Schalley, Integrative self-sorting: construction of a cascade-stoppered hetero[3]rotaxane, *J. Am. Chem. Soc.*, 2008, **130**, 13852–13853.
- 39 W. Jiang and C. A. Schalley, Molecular recognition and self-assembly special feature: Integrative self-sorting is a programming language for high level self-assembly, *Proc. Natl. Acad. Sci. U. S. A.*, 2009, **106**, 10425–10429.
- 40 X. Fu, Q. Zhang, S. J. Rao, D. H. Qu and H. Tian, One-pot synthesis of a [c2]daisy-chain-containing hetero[4]rotaxane via a self-sorting strategy, *Chem. Sci.*, 2016, **7**, 1696–1701.
- 41 S. J. Rao, Q. Zhang, J. Mei, X. H. Ye, C. Gao, Q. C. Wang, D. H. Qu and H. Tian, One-pot synthesis of hetero[6]rotaxane bearing three different kinds of macrocycle through a self-sorting process, *Chem. Sci.*, 2017, **8**, 6777–6783.
- 42 W. Jiang, A. Schäfer, P. C. Mohr and C. A. Schalley, Monitoring self-sorting by electrospray ionization mass spectrometry: formation intermediates and error-correction during the self-assembly of multiply threaded pseudorotaxanes, *J. Am. Chem. Soc.*, 2010, **132**, 2309–2320.
- 43 H. V. Schröder, H. Hupatz, A. J. Achazi, S. Sobottka, B. Sarkar, B. Paulus and C. A. Schalley, A Divalent Pentastable Redox-Switchable Donor-Acceptor Rotaxane, *Chem. – Eur. J.*, 2017, **23**, 2960–2967.
- 44 H. V. Schröder, A. Mekic, H. Hupatz, S. Sobottka, F. Witte, L. H. Urner, M. Gaedke, K. Pagel, B. Sarkar, B. Paulus and



- C. A. Schalley, Switchable synchronisation of pirouetting motions in a redox-active [3]rotaxane, *Nanoscale*, 2018, **10**, 21425–21433.
- 45 H. Hupatz, M. Gaedke, H. V. Schröder, J. Beerhues, A. Valkonen, F. Klautzsch, S. Müller, F. Witte, K. Rissanen, B. Sarkar and C. A. Schalley, Thermodynamic and electrochemical study of tailor-made crown ethers for redox-switchable (pseudo)rotaxanes, *Beilstein J. Org. Chem.*, 2020, **16**, 2576–2588.
- 46 M. Gaedke, H. Hupatz, H. V. Schröder, S. Suhr, K. F. Hoffmann, A. Valkonen, B. Sarkar, S. Riedel, K. Rissanen and C. A. Schalley, Dual-stimuli pseudorotaxane switches under kinetic control, *Org. Chem. Front.*, 2021, **8**, 3659–3667.
- 47 I. R. Hanson, D. L. Hughes and M. R. Truter, Crystal and molecular structure of 6,7,9,10,12,13,20,21,23,24,26,27-dodecahydrodibenzo[b,n][1,4,7,10,13,16,19,22]octaoxacyclo-tetracosin (dibenzo-24-crown-8), *J. Chem. Soc., Perkin Trans. 2*, 1976, 972.
- 48 H. V. Schröder, S. Sobottka, M. Nössler, H. Hupatz, M. Gaedke, B. Sarkar and C. A. Schalley, Impact of mechanical bonding on the redox-switching of tetrathiafulvalene in crown ether-ammonium [2]rotaxanes, *Chem. Sci.*, 2017, **8**, 6300–6306.
- 49 S. Grimme, J. G. Brandenburg, C. Bannwarth and A. Hansen, Consistent structures and interactions by density functional theory with small atomic orbital basis sets, *J. Chem. Phys.*, 2015, **143**, 054107.
- 50 A. Klamt and G. Schüürmann, COSMO: a new approach to dielectric screening in solvents with explicit expressions for the screening energy and its gradient, *J. Chem. Soc., Perkin Trans. 2*, 1993, 799–805.
- 51 F. Nicoli, M. Baroncini, S. Silvi, J. Groppi and A. Credi, Direct synthetic routes to functionalised crown ethers, *Org. Chem. Front.*, 2021, **8**, 5531–5549.

